Geophysical Research Letters

Supporting Information for

The distribution and characterization of strike-slip faults on Enceladus

Emily S. Martin

Department of Geological Sciences, University of Idaho, 875 Perimeter Drive MS 3022, Moscow, Idaho 83844-3022

E. S. Martin now at Center for Earth and Planetary Studies, National Air and Space Museum, Smithsonian Institution, Washington, D. C. 20560

Contents of this file

Introduction

The following supplemental information outlines detailed discussions on Riedel shears, methods for mapping strike-slip faults, calculations and equations for stress calculations, stress modeling, and additional figures relevant to the main text.

Text S1.

En echelon fractures and Riedel shears

En echelon cracks are a type of a group of fractures called Riedel shears, which are secondary fractures that form in response to underlying shear fractures [*Riedel*, 1929] (Sup. Fig 1). There are a variety of Riedel shears, most notably R-shears and R'-shears, conjugate fractures with synthetic and antithetic motion, respectively. Other Riedel shears include:

synthetic P-shears that form at low angles to the parent crack and 2) T-fractures, which are tension fractures that form at 45° to the parent crack (Sup. Fig. 1); the sense of step of the T-fractures is opposite to the shear direction of the underlying fault. En echelon cracks in this scenario are mode I features forming perpendicular to the direction of local maximum horizontal tension (σ_1), and parallel to the local maximum horizontal compression (σ_3). These echelon cracks step in the opposite direction from the sense of slip: left-stepping en echelon cracks result from right-lateral strike-slip motion, and right-stepping cracks result from left-lateral motion.

Figure S1. Riedel Shears.

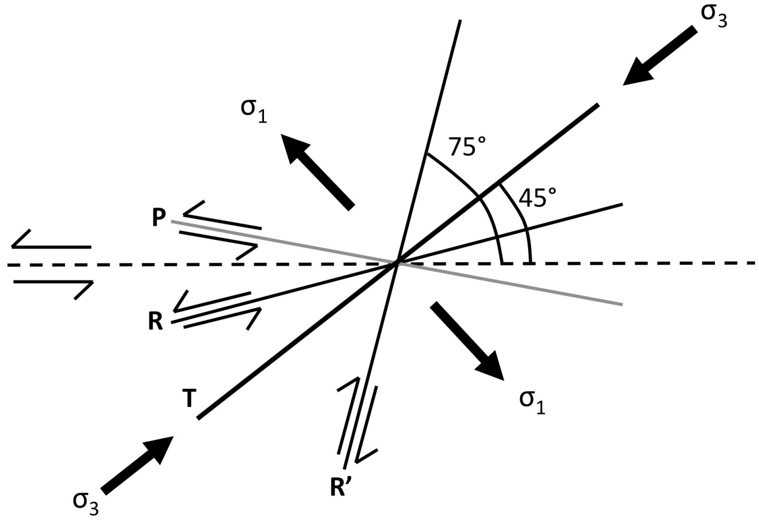

Figure S1: Schematic of Riedel Shears forming from a left-lateral strike-slip fault (dashed horizontal line). P, R, R', and T are types of Riedel Shears described in Text S1. We interpret observed arrays of en echelon cracks as T cracks which are at a 45° angle to the strike of the subsurface strike-slip fault (After Twiss & Moore, 1992).

Text S2.

Strike-slip fault mapping

Mapping was completed on the global mosaic and north polar mosaic of Enceladus [*Roatsch et al.,* 2013] from the NASA Planetary Data System's (PDS) Imaging Node Planetary Image Atlas. The mosaic has a resolution of 110 m/pixel, which is lower than many of the individual images used to create the mosaic. To supplement the basemap, individual high-resolution images were retrieved from the PDS and processed using the Integrated Software for Imagers and Spectrometers (ISIS) developed by the United States Geological Survey. Images were selected based on their resolution (40-200m/pixel), which included overlapping images that provide all lighting geometries available for Enceladus within the Cassini PDS dataset. The incidence angles for all the images within the PDS dataset (Figure S2) show a wide range with only a few images with incidence angles <15°, which do not optimize observations of surface morphologies. Images were imported into an ArcGIS environment where the combination of the global mosaic and individual high-resolution images allowed for the most detailed analysis of strike-slip faults. We performed a survey of strike-slip faults excluding the SPT; occasional offsets have been observed within the SPT [*Patthoff & Kattenhorn,* 2011] but were not comparable to the scale of strike-slip faulting observed elsewhere on Enceladus (image resolutions within the SPT can be as low as <10 meters per pixel), and were therefore not included in this work.

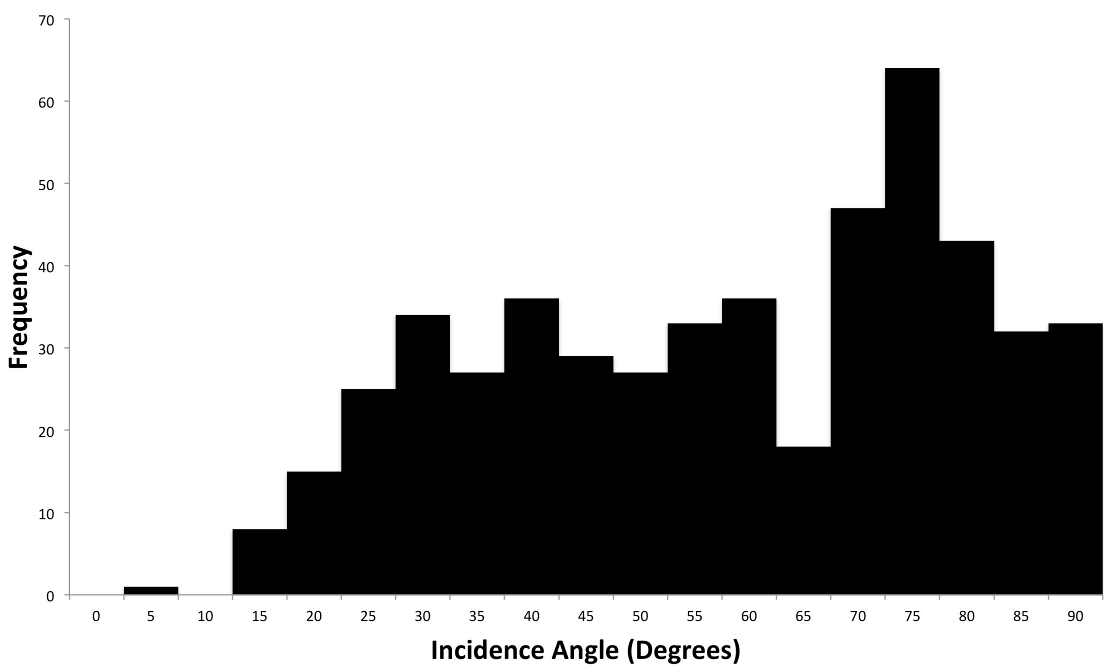

Figure S2: A histogram of the range of incidence angles from the suite of images downloaded from the PDS and used to supplement the global mosaic basemap by *Roatsch et al.,* [2013].

Text S3.

Inferring a normal-vs.-shear stress ratio from observations

A stress intensity factor (K_I, K_{II}, and K_{III}) is the magnitude of a stress local to the fracture tip: K_I, K_{II}, and K_{III} are measures of the magnitude of stress modes I, II, or III, respectively. The ratio of

$K_{(II\ or\ III)}/K_I$ represents the ratio of the relative amounts of mode II or III shearing to opening of a fracture, and this ratio can be derived from observations of tailcrack and en echelon crack angles. The tailcrack angle can be mathematically related to the ratio of the shear stress to the normal stress (σ_s/σ_n) [*Erdogan & Sih,* 1963; *Pollard & Segall,* 1987; *Willemse & Pollard*, 1998], and K_{II}/K_I [see *Groenleer & Kattenhorn,* 2008]. Similarly, en echelon crack angles are related to K_{III}/K_I [*Pollard et al.,* 1982], and can be related back to σ_s/σ_n. To calculate the relative amounts of opening and shearing at tailcracks and en echelon cracks the K_{II}/K_I and K_{III}/K_I ratios are used (Table S1). After *Groenleer & Kattenhorn,* [2008]:

$$\frac{K_{II}}{K_I} = \frac{sin\left(\frac{\theta}{2}\right)\times cos\left(\frac{\theta}{2}\right)}{3sin^2\left(\frac{\theta}{2}\right)-1} \qquad (1)$$

where θ is the tailcrack angle.

Similarly, for dilational en echelon surface fractures (interpreted here as a Reidel T-fractures) forming as the result of an underlying shear fracture, the en echelon crack angle β (Fig. 2c, d), can be used to calculate the ratio [*Pollard et al.,* 1982]:

$$\frac{K_{III}}{K_I} = tan(2\beta)\times\left(\frac{1}{2}-\nu\right) \qquad (2)$$

where ν is Poisson's ratio (see Table S2 for values used).

Equation 2 is only relevant if the normal stress acting on the primary crack is tensile (i.e., experiencing a component of dilation). The K_{II}/K_I and K_{III}/K_I ratios from equations 1 and 2 are based on the observed geometries of fractures related to strike-slip faults (Table S1). A negative normal stress indicates a compressive stress, which would require reassessment to determine if the observed en echelon cracks match other expected geometries for the sense of shear, such as for R, R', or P shears (Fig. S1) [*e.g., Riedel,* 1929].

Text S4.

Inferring a normal-vs.-shear stress ratio from stress models

We used SatStressGUI [*Kay,* 2010] based on SatStress, an open source program for calculating global stresses in the ice shell of a tidally-deforming moon [*Wahr et al.,* 2009], to derive a global stress field due to NSR. SatStressGUI uses a 4-layer model to represent the satellite interior: upper and lower ice shells, a global subsurface ocean, and a rocky core. We selected a NSR period of 1 Myr, which allowed sufficient stress to accrue to enable fracturing prior to the viscoelastic relaxation of such stresses, and consistent with previous work [*Kay*, 2010]. We selected rheological parameters for low temperature ice (Table S2) for each of the four layers. SatStressGUI adopts a tension positive sign convention and was used to calculate σ_1, σ_3, and α (the orientation of σ_1 measured clockwise form due north (0°)) at a coordinate located at the center of the trace of the strike-slip fault. The Mohr equations:

$$\sigma_n = \frac{\sigma_1+\sigma_3}{2} + \frac{\sigma_1-\sigma_3}{2} cos(2\Theta) \tag{3}$$

$$\sigma_s = \frac{\sigma_1-\sigma_3}{2} sin(2\Theta) \tag{4}$$

relate the magnitude of the principal stresses (from SatStressGUI) to the amount of normal and shear stress on the fault. Θ is the angle between α (the angle between north and σ_1) and a vector normal to the fault.

Table S1.

A summary of the results from observed en echelon crack and tailcrack angles. The NSR longitude is the point in the NSR stress field where $\sigma_s/\sigma_n \approx K_{II(III)}/K_I$. Faults highlighted in gray indicate those that are consistent with formation within an NSR stress field. Faults [7] and [29] appear twice, because there are two longitudes within the NSR stress field where $\sigma_s/\sigma_n \approx K_{II(III)}/K_I$.

		Fault ID	Type	NSR Long.	Center Lat.	Crack Angle	Obs. Slip Sense	NSR Slip Sense	$\frac{\sigma_s}{\sigma_n}$	$\frac{K_{II}}{K_I}$	$\frac{K_{III}}{K_I}$
Secondary Crack Types	Tail-crack	1	Primary	-81.18	-26.5	50°	Left	Left	-0.6	-0.82	-
		2	Reactivated	-65.65	17.51	47°	Left	Left	-0.39	-0.69	-
		3	Primary	-91.24	21.91	45°	Right	Left	-0.70	-0.63	-
		28	Boundary	46.79	-43.58	19°	Left	Right	-0.30	-0.18	-
	En Echelon crack	5	Boundary	-17.4	-8.6	28°	Left	Right	0.46	-	0.25
		6	Primary	-	-2.15	12°	Left	-	-	-	0.07
		7	Primary	159.87	22.57	32°	Right	Left	0.34	-	0.35
		7	Primary	-20.13	22.57	32°	Right	Left	0.34	-	0.35
		8	Reactivated	170.13	35.85	28°	Right	Left	0.25	-	0.25
		18	Primary	-	-29.21	40°	Right	-	-	-	0.96
		21	Boundary	-36.86	18.2	29°	Right	Left	0.35	-	0.27
		23	Primary	-40.62	42.42	20°	Right	Left	0.14	-	0.14
		24	Primary	-59.56	40.98	11°	Right	Left	0.28	-	0.07
		27	Reactivated	53.71	-43.82	16°	Left	Right	0.13	-	0.11
		29	Reactivated	167.25	-20.14	17°	Left	Right	0.13	-	0.11
		29	Reactivated	-12.25	-20.14	17°	Left	Right	0.13	-	0.11
Other Strike-slip Faults	Stepped Segments	12	Boundary	-	33.72	-	Right	-	-	-	-
		16	Reactivated	-	-25.0	-	Left	-	-	-	-
		32	Reactivated	-	-32.27	-	Left	-	-	-	-
	Shear Zone	11	Reactivated	-	-28.11	-	Left	-	-	-	-
		14	Reactivated	-	-12.39	-	Right	-	-	-	-
		15	Boundary	-	-42.86	-	Right	-	-	-	-
		25	Primary	-	59.76	-	Left	-	-	-	-

Table S2.

Parameters used to calculate point stresses at Enceladus's surface using SatStressGUI [*Wahr et al.*, 2009; *Kay*, 2010]. ρ is density, G is the shear modulus, λ is the Lamé Parameter, η is the viscosity, E is Young's Modulus, and ν is Poisson's Ratio. Rheological properties are consistent with previous work [*Olgin et al.*, 2011; *Smith-Konter & Pappalardo* 2008; *Nimmo et al.*, 2007].

	ρ(kg/m^3)	G (Pa)	λ (Pa)	Thickness (m)	η (Pa·s)	E	ν (Pa)
Upper Ice Shell	917	3.5x10^9	6.8x10^9	2x10^3-8x10^3	1x10^{23}	9.3107x10^9	3.301x10^{-1}
Lower Ice Shell	917	3.5x10^9	6.8x10^9	2.2x10^4-7.8x10^4	1x10^{17}	9.3107x10^9	3.301x10^{-1}
Ocean	1000	-	2x10^9	1x10^4- 7.2x10^4	-	-	-
Core	3500	1x10^{12}	4x10^{10}	1.56x10^5	-	-	-

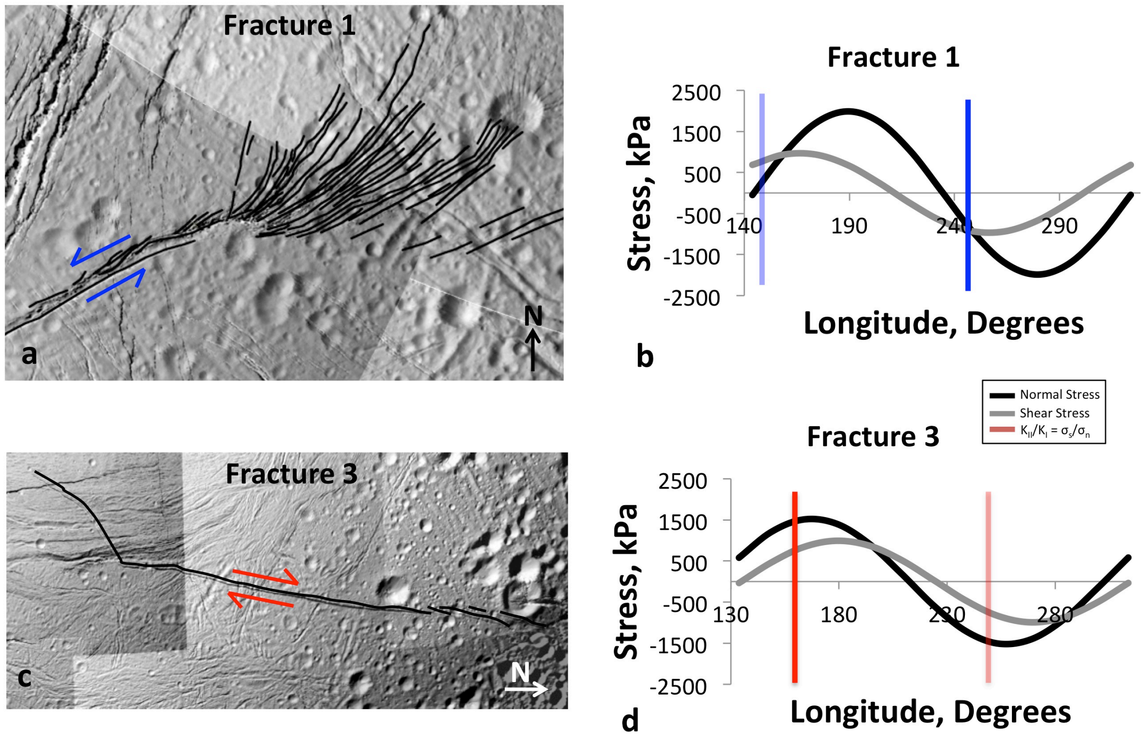

Figure S3: a. Strike-slip fault centered at 143°E and 26°S with a tailcrack angle of 50° and a K_{III}/K_I=0.83 (Table S1). This fault [1] likely formed due to NSR. **b.** Plot of normal (black) and shear (gray) stress resolved in an NSR stress field. Vertical bar indicates the longitudes at which $K_{III}/K_I=\sigma_s/\sigma_n$. **c.** Strike-slip fault centered at 133°E and 21°N with a tailcrack angle of 45° and K_{II}/K_I=0.63. This fault [3] likely formed due a stress mechanism other than NSR. **d.** Plot of normal and shear stress for [3]. Vertical bar indicates the longitudes at which $K_{II}/K_I=\sigma_s/\sigma_n$. Faults [1] and [3] are resolved in an NSR stress field at the longitudes indicated by vertical bars in **b** and **d** in Figure S3.

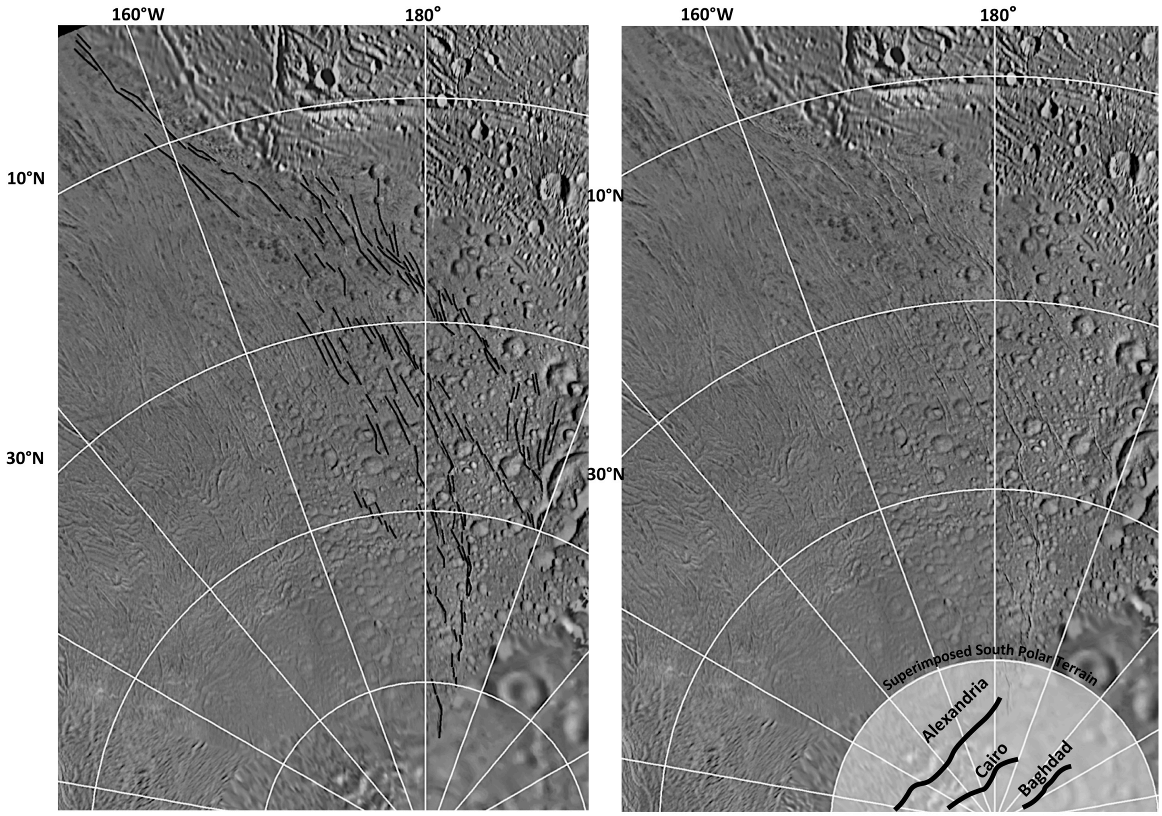

Figure S4: Right-lateral shear zone associated with [25] traced into the north polar regions. North polar mosaic from *Roatsch et al.,* [2013]. The south polar terrain is superposed on the north polar region to show the relationship of this region to the opening direction of the tiger stripes.

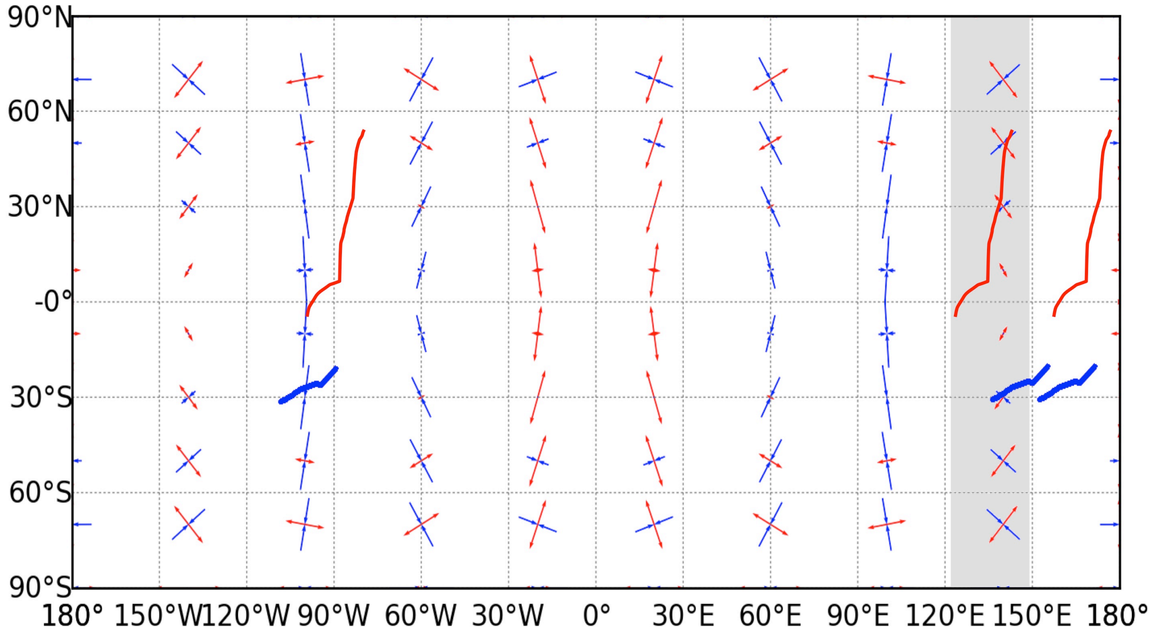

Figure S5: An NSR stress field shown with fault [1] (blue) and fault [3] (red). The present day location of each fracture is indicated by the gray band. The other two pairs of fractures are longitudes where $K_{II(III)}/K_{I}=\sigma_s/\sigma_n$ due to NSR. Blue arrows marks indicate the direction of maximum compression. Red arrows indicate the direction of maximum tension. The locations of faults [1] and [3] outside of the grey area correspond to the longitudes indicated by the vertical bars in Figures 3**b** & **d**.

References in Supplemental Information

Erdogan, F., and C. G. Sih, (1963), On the crack extension in plates under plane loading and transverse shear. *J. Bas. Eng.*, 85, 519-527. doi:10.1115/1.3656897.

Groenleer, J. M., and S. A. Kattenhorn, (2008), Cycloid crack sequences on Europa: Relationship to stress history and constraints on growth mechanics based on cusp angles. *Icarus,* 193, 158-181. doi:10.1016/j.icarus.2007.08.032.

Kay, J. P., (2010), The case for recent tectonic activity on Jupiter's moon Europa. Moscow, ID: Unpublished masters thesis.

Nimmo, F., J. R., Spencer, R. T. Pappalardo, M. E. Mullen, (2007), Shear heating as the origin of the plumes and heat flux on Enceladus. *Nature*, 447, 289-291. doi:10.1038/nature05783.

Olgin, J. G., B. R. Smith-Konter, R. T. Pappalardo, (2011), Limits of Enceladus's ice shell thickness from tidally driven tiger stripe shear failure. *Geophys. Res. Let.,* 38, L02201. doi:10.1029/2010GL044950.

Patthoff, D. A., & S. K. Kattenhorn, (2011), A fracture history on Enceladus provides evidence for a global ocean. *Geophys. Res. Let.*, 38, L18201. doi:10.1029/2011GL048387.

Pollard D. D., P. Segall, P. Delaney, (1982), Formation and interpretation of dilatant echelon cracks. *Bull. Geol. Soc. Am.* 93, 1291-1303. doi:10.1130/0016-7606(1982)93<1291:FAIODE>2.0.CO;2.

Pollard, D. D., and P. Segall, (1987), Theoretical displacements and stresses near fractures in rock: with applications to faults, joints, veins, dikes, and solution surfaces. *In,* Fracture mechanics of rock, B. K., Atkinson eds. Academic Press, London. 277-349.

Riedel, W., (1929), Zur mechanic geologischer Brucherscheinungen (Ein Beitrag zum Problem der Fiederspatten). *Zentbl. Miner. Geol. Paläeont. Abh.* B, 354-368.

Roatsch, Th., E. Kersten, A. Hoffmeister, M. Wählisch, K.-D. Matz, C. C. Porco, (2013), Recent improvements of the Saturnian satellites atlases: Mimas, Enceladus, and Dione. *Planetary and Space Science*, 77, 118-125. doi:10.1016/j.pss.2012.02.016.

Smith-Konter, B., and R. T. Pappalardo, (2008), Tidally driven stress accumulation and shear failure of Enceladus's tiger stripes. *Icarus*, 198, 435-451. doi:10.1016/j.icarus.2008.07.005.

Twiss, R. J. and E. M. Moores (1992). Structural Geology, 174 pp., W. H. Freeman and Company, New York, NY.

Wahr, J., Z. A. Selvens, M. E. Mullen, A. C. Barr, G. C. Collins, M. M. Selvans, R. T. Pappalardo, (2009), Modeling stresses on satellites due to nonsynchronous rotation and orbital eccentricity using gravitational potential theory. *Icarus, 200(1)*, 188-206, doi:10.1016/j.icarus.2008.11.002.

Willemse, E. J. M., D. C. P. Peacock, A. Aydin, (1997), Nucleation and growth of strike-slip faults in limestone from Somerset, U.K.. *J. Struct. Geol*. 19, 1461-1477. doi:10.1016/S0191-814(97)00056-4.